RSC Advances

PAPER

View Article Online
View Journal | View Issue

Cite this: *RSC Adv.*, 2019, **9**, 23888

Controllable synthesis of multi-shelled $NiCo_2O_4$ hollow spheres catalytically for the thermal decomposition of ammonium perchlorate

Wenchao Zhang, *[a] Bin Jiang,[a] Xiaohang Ma,[a] Jiaxin Wang,[a] Jiaqi Liu,[b] Runhui Wu,[c] Zilong Zheng,[a] Jingping Liu[a] and Kefeng Ma*[d]

Received 22nd May 2019
Accepted 17th July 2019

DOI: 10.1039/c9ra03865e

rsc.li/rsc-advances

The compatible catalytic structure of $NiCo_2O_4$ was modified into multi-shelled hollow spheres by one-pot synthesis, followed by heat treatment. X-ray diffraction (XRD), scanning electron microscopy (SEM), transmission electron microscopy (TEM), and Brunauer–Emmet–Teller (BET) and N_2 adsorption–desorption approaches were used for the characterizations of nanoparticles and multi-shelled hollow porous structures and the morphologies and crystal structures of these hollow spheres, respectively. Differential scanning calorimetry (DSC) was adopted for comparing the thermal decomposition performances of ammonium perchlorate (AP) catalyzed by adding different contents of multi-shelled $NiCo_2O_4$ hollow spheres. Impressively, the experimental results showed that the $NiCo_2O_4$ hollow spheres exhibited more excellent catalytic activity than $NiCo_2O_4$ nanoparticles as a result of their large specific surface areas, good adsorption capacity and many active reduction sites. The decomposition temperature of AP with multi-shelled $NiCo_2O_4$ hollow spheres could be reduced up to 322.3 °C from 416.3 °C. Furthermore, a catalytic mechanism was proposed for the thermal decomposition of AP over multi-shelled $NiCo_2O_4$ hollow spheres based on electron transfer processes.

1. Introduction

Solid propellants are required to have favorable combustion performances and design compatibility for applications as rocket fuels, which is one of the research hotspots in space propulsion projects.[1–4] AP as a high-energy component accounts for 60–90% of the solid propellant content. Therefore, its combustion performance is important for further considerations in order to understand its thermal decomposition behavior.[5] The regulation in its thermal decomposition temperature is quite significant for both ignition delay time and boosting the burning rate.[6] From this point of view, a number of transition metal oxides and complex compounds with satisfactory performances were synthesized.[7–12] However, the problems of agglomeration, slow mass transfer[5] and improvement in thermal decomposition temperatures still need scientific attention. Morphological and microstructural modifications can be conducted to achieve highly efficient performances.[13–15] This work is expected to help find more details on a simple and quick preparation process, highly exposed specific surface area, fast mass transportation and numerous catalytic active sites.

Hollow sphere nanocomposites with a controlled number of shells have aroused widespread concern in the past several years because of their special structures, due to which they are potential materials for applications in photocatalysis,[16–18] drug delivery vehicles,[19–21] storage systems and energy conversion.[22–26] In the latest reports, many scientists have made considerable efforts to fabricate hollow spheres with multiple shells. For example, Lai *et al.* reported the preparation of multi-shelled hollow microspheres (MFe_2O_4; M = Cd, Co and Zn) by means of sequential templates.[27] Lou and co-workers adopted carbonaceous spheres as hard templates to prepare $ZnCo_2O_4$ and $CoMn_2O_4$ hollow spheres with complex internal structures using a "penetration-solidification-annealing" treatment.[28] Wang *et al.* prepared shell-controllable $CoFe_2O_4$ (CFO) hollow microspheres using a hydrothermal–calcination method.[29] Li *et al.* reported the synthesis of hollow layered double hydroxides (LDHs) with polystyrene beads as the template.[30] Yao *et al.* successfully synthesized multi-shelled hollow spheres *via* a sacrificial template using polystyrene divinyl benzene spheres.[31] Despite these innovative advances, the majority of these reported methods are only suitable for specific multi-shelled hollow spheres.[28,32,33] Furthermore, these reported methods cannot realize a precise control of the number of shells and are difficult to be applied for mass production as well.[27,34]

[a]*School of Chemical Engineering, Nanjing University of Science and Technology, Nanjing, 210094, China*
[b]*The First Academy of China Aerospace Science and Technology Corporation, Beijing, 100048, China*
[c]*National Key Laboratory on Science and Technology on Test Physics and Numerical Mathematics, Beijing, 100076, China*
[d]*School of Environmental and Biological Engineering, Nanjing University of Science and Technology, Nanjing, 210094, China*

Therefore, it is highly desirable to develop a universal method to construct hollow spheres of multiple compositions with a controllable number of shells.

Binary transition metal oxides (BTMOs) are more susceptible to electron transfer between multiple cations due to their more unfilled electron orbitals when compared with single transition metal oxides. As a result, they can exhibit excellent catalytic performances under the synergistic effect of composite metal oxides.[35] In this study, shell-controllable $NiCo_2O_4$ hollow spheres were successfully synthesized by a simple and rapid preparation process. By the direct introduction of metal salts into aqueous glucose solutions before a hydrothermal treatment, remarkable properties such as large specific surface area, fast mass transfer and multiple catalytic active sites were achieved. As far as we know, the reported research on $NiCo_2O_4$ hollow spheres as a catalyst to promote the thermal decomposition of AP is scarce. Besides, the structure and morphology of the as-prepared $NiCo_2O_4$ hollow spheres were characterized to propose a formation mechanism. Their catalytic performances for the thermal decomposition of AP were examined using DSC in order to suggest a catalytic mechanism.

2. Experimental section

2.1 Materials

The chemical reagents $Co(NO_3)_2 \cdot 6H_2O$, $Ni(NO_3)_2 \cdot 6H_2O$, glucose, diethylene glycol, deionized water, ethanol and NH_4ClO_4 were purchased from Sinopharm Chemical Reagent Co., Ltd. All chemicals were of analytical grade and used without further purification during all synthetic procedures.

The X-ray diffraction (XRD) patterns of the as-prepared samples were obtained on Bruker D8 Advance equipped with monochromatized Cu Kα radiation (λ = 0.15406 nm). The morphologies were characterized by scanning electron microscopy (SEM, Hitachi S-4800) and transmission electron microscopy (TEM, (JEOL) JEM-2100). Nitrogen adsorption/desorption isotherms of the samples at −196 °C were described using a Micromeritics TriStar II 3020 porosimetry analyzer. Pore size distributions and surface areas were calculated according to the Barrett–Joyner–Halenda (BJH) and Brunauer–Emmett–Teller (BET) methods, respectively. The thermal decomposition process of AP was measured by a differential scanning calorimeter (DSC, Mettler Toledo) under the nitrogen flow of 20 mL min^{-1} at a heating rate of 20 °C min^{-1} from 50 °C to 500 °C.

2.2 Synthesis of the multi-shelled $NiCo_2O_4$ hollow spheres

Multi-shelled $NiCo_2O_4$ hollow spheres were synthesized as follows: in general, certain amounts of glucose, $Co(NO_3)_2 \cdot 6H_2O$ and $Ni(NO_3)_2 \cdot 6H_2O$ were dissolved in 60 mL water at a molar ratio of 3 : 4 : 2. After vigorous stirring for 30 min, the resultant uniform and transparent solution was transferred to a 100 mL Teflon-lined autoclave for a 6 h hydrothermal reaction at 180 °C. The precursors were then collected after washing with ethanol and water several times and dried in a vacuum oven overnight. The double-shelled hollow spheres were finally obtained after the precursor was heated at a rate of 10 °C min^{-1} up to 500 °C and then maintained at this temperature for 3 h in a muffle furnace under air. The number of shells could be controlled by the regulation of the heating rate during calcination. For example, the triple-shelled $NiCo_2O_4$ hollow spheres can be achieved at the heating rate of 5 °C min^{-1}. The preparation of single-shelled $NiCo_2O_4$ is as follows: first, we dissolved 5.4 g of glucose in 60 mL of water to obtain a 0.5 M glucose solution. Second, the resulting solution was transferred to a 100 mL Teflon-lined autoclave for a 6 h reaction at 180 °C. Third, the obtained carbon spheres were immersed in a mixture of $Ni(NO_3)_2$ and $Co(NO_3)_2$ (molar ratio, 1 : 2) at a concentration of 2 M for 20 min. Finally, the single-shelled hollow spheres were obtained after the precursor was heated at a rate of 20 °C min^{-1} up to 500 °C and then maintained at this temperature for 3 h in a muffle furnace under air.

2.3 Measurements of catalytic activities

For the evaluation of the catalytic performance of the as-obtained samples on the thermal decomposition of AP, the mixture of either $NiCo_2O_4$ nanoparticles, single-shelled, double-shelled, or triple-shelled $NiCo_2O_4$ hollow sphere powder with AP was ground in a glass mortar for 30 min to ensure the homogeneous dispersion of the as-obtained samples. The mass ratio of AP : sample was taken as 49 : 1. The thermal decomposition of neat AP without $NiCo_2O_4$ was also reviewed for comparison. Meanwhile, a variety of mixed samples of AP and as-obtained $NiCo_2O_4$ were investigated in different weight ratios. The catalytic effect of the $NiCo_2O_4$ hollow spheres on AP was evaluated by the same analyses for obtaining the decomposition temperature of AP.

3. Results and discussions

3.1 Physical characterizations

The crystal phases of the $NiCo_2O_4$ nanoparticles and $NiCo_2O_4$ hollow spheres were inspected by XRD, as revealed in Fig. 1. All $NiCo_2O_4$ nanocomposites, which were synthetized under different experimental conditions, exhibited similar XRD patterns, where all the diffraction peaks of (111), (220), (311),

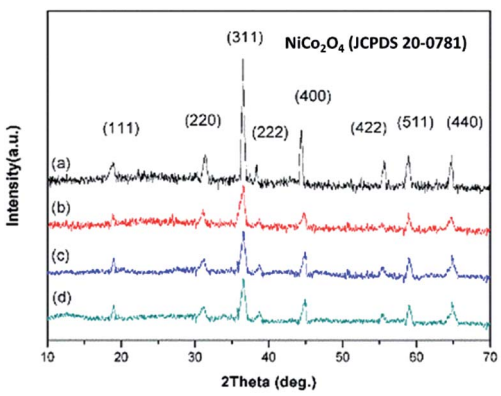

Fig. 1 The XRD patterns of (a) $NiCo_2O_4$ nanoparticles and (b) single-shelled, (c) double-shelled, and (d) triple-shelled $NiCo_2O_4$ hollow spheres.

(222), (400), (422), (511) and (440) fitted well with the standard diffraction data of $NiCo_2O_4$ (JCPDS 20-0781).[36] Furthermore, the absence of additional peaks indicated that the precursor completely transformed into $NiCo_2O_4$ after the annealing treatment. The clearly defined and strong peaks also revealed the crystallinity and high purity of the produced $NiCo_2O_4$ samples.

3.2 Formation mechanism

The formation procedure of the double-shelled $NiCo_2O_4$ hollow spheres is illustrated in Fig. 2. At the primary stage of the reaction, first, the glucose dehydration reaction produces oligosaccharides and aromatic compounds. Then, the oligosaccharides are dehydrated at a higher temperature to cause intermolecular crosslinking and finally, the resulting nuclei grow to form carbon spheres with reactive functional groups.[37] The metal salt is captured into the carbon sphere during this process, forming a composite structural material, whose components are mainly carbonaceous particles and metal salt hydrates. The precursors for the double-shelled $NiCo_2O_4$ hollow spheres were fabricated by means of a chemically initiated dehydration process using the carbonaceous particles and metal salt hydrates as starting materials. Subsequently, on increasing the calcination temperature, the metal oxide hydrates began to crystallize on the outermost shell before the carbonaceous spheres contraction. When the calcination temperature increased up to *ca.* 350 °C, the metal oxide hydrates could speed up crystallization to form a thermally stable shell of metal oxide before the carbonaceous layer started to burn. Finally, as the annealing temperature rose to a critical value (*e.g.*, 350–500 °C), the combustion of the carbonaceous layer provided enough energy for the separate between cores and shells.[33] Therefore, the hollow spheres with a controllable number of layers can be obtained *via* this facile one-pot approach. It is noteworthy here that this protocol should be expected to be qualified for a variety of metal oxides to realize multishell formation based on the templates of these carbonaceous spheres.

The SEM and TEM images are displayed in Fig. 3 for the precursors of carbon spheres and hollow multi-shelled microspheres, which were prepared at different calcination temperatures as high as 500 °C. As observed from Fig. 3a and d, the prepared precursors of the carbon spheres have a smooth

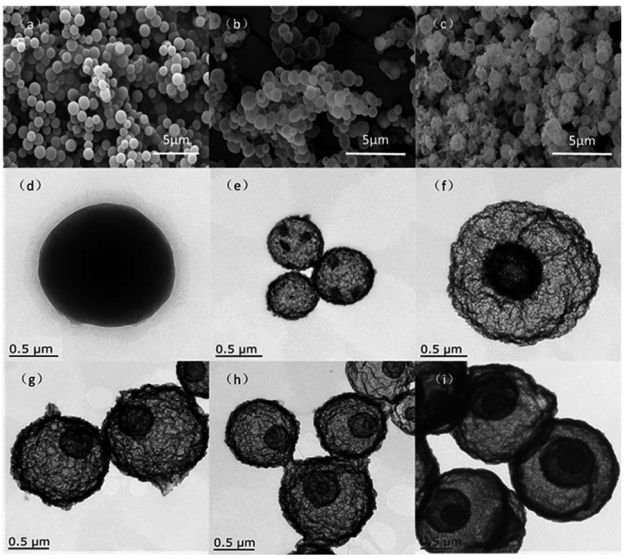

Fig. 3 The SEM images of (a) the precursors of the $NiCo_2O_4$ hollow spheres, (b) single-shelled $NiCo_2O_4$ and (c) double-shelled $NiCo_2O_4$ hollow spheres; the TEM images of (d) the precursors of the $NiCo_2O_4$ hollow spheres, (e) single-shelled $NiCo_2O_4$ hollow spheres, (f and g) double-shelled $NiCo_2O_4$ hollow spheres, (h and i) triple-shelled $NiCo_2O_4$ hollow spheres.

surface and a uniform particle size. As a whole, these precursors demonstrate good configuration with few grain boundaries and regional defects microscopically and thus, they can be adopted as good templates for hollow spheres. It can be seen from Fig. 3b and e that the surface of the single-shell hollow spheres is smooth and transparent. Double- and triple-shelled $NiCo_2O_4$ hollow spheres, obtained by a change in the heating rate during calcination, are displayed in Fig. 3c and f–i. Their surfaces have irregular pleats, which may be caused by the uneven distribution of metal salts inside the carbon spheres. This morphology also helps increase the number of surface activation sites in the sample.

The as-synthesized samples were investigated by physisorption of N_2 and the resulting curves are exhibited in Fig. 4. It can be obviously seen that the isotherm has the characteristics of a "type II" isotherm with H3 hysteresis loops (Fig. 4a).[38–40] On the basis of the BET method, the specific surface areas of the single- and triple-shelled $NiCo_2O_4$ hollow spheres were calculated to be 48.6 $m^2\ g^{-1}$ and 88.2 $m^2\ g^{-1}$, respectively. Besides, the specific surface area of the double-shelled $NiCo_2O_4$ hollow

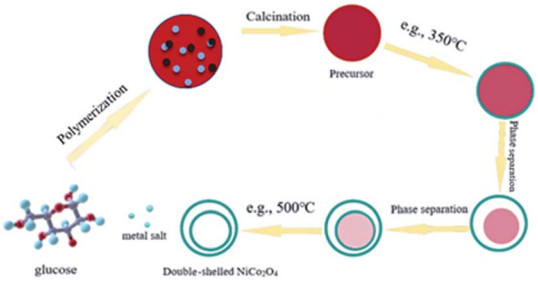

Fig. 2 The schematic illustration for the formation of double-shelled $NiCo_2O_4$ hollow spheres.

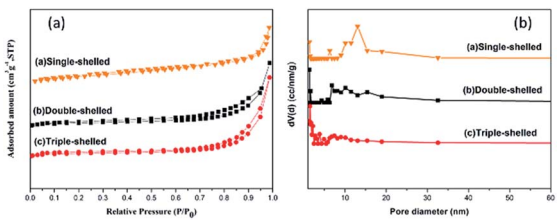

Fig. 4 (a) The nitrogen adsorption–desorption isotherms and (b) pore-size distributions of $NiCo_2O_4$ hollow spheres with different shell numbers.

spheres was surprisingly 102.7 m^2 g^{-1}, which was the largest value among all the values of the hollow spheres investigated here. The pore sizes of the three kinds of $NiCo_2O_4$ hollow spheres were mainly between 2–4 nm and 8–20 nm, as displayed in Fig. 4b. The formation of pores (2–4 nm) may be due to particle accumulation, while the large pores (8–20 nm) are supposed to be caused primarily by gas diffusions during the calcination process. The pores (8–20 nm) can provide a pathway for gas emission. From Fig. 4b, it can be seen that the pores become increasingly smaller from single- to double- to triple-shelled $NiCo_2O_4$, which may be attributed to the lower heating rate. The macropores of hollow spheres are highly conducive for gaseous intermediates to enter, due to which plenty of active sites will be provided for their electron transfer.

3.3 Catalytic performances of multi-shelled $NiCo_2O_4$ hollow spheres towards AP

The DSC curves are displayed in Fig. 5 for neat AP and the mixtures of AP with $NiCo_2O_4$ nanoparticles or $NiCo_2O_4$ hollow spheres with different shell numbers. The thermal decomposition process of neat AP can be split into three steps as follows (Fig. 5a): the first stage is an endothermic process for the crystalline transformation of AP from an orthorhombic to a cubic phase, and its transition temperature is 240–250 °C with its peak temperature of 242.0 °C; this is in agreement with the reported data.[41–43] On increasing the temperature, the decomposition of neat AP can exothermically suffer one low-temperature decomposition (LTD) and one high-temperature decomposition (HTD) process, which can begin at 282.0 °C and 354.0 °C with the peak temperatures of 306.4 °C and 416.3 °C, respectively. At last, AP can be completely decomposed to produce volatile products such as HCl, H_2O, Cl_2, O_2, NO, N_2O and NO_2.[44] The HTD temperature of AP can be reduced by 36.4 °C due to the presence of $NiCo_2O_4$ nanoparticles (Fig. 5b). This indicates that the transition metal oxides can exert a positive effect on the decomposition of AP. Compared with $NiCo_2O_4$ nanoparticles, the $NiCo_2O_4$ hollow spheres exhibited stronger catalytic activities. The single-shelled $NiCo_2O_4$ hollow spheres could decrease the HTD temperature of AP to 366.4 °C (Fig. 5c), but the double-shelled hollow spheres caused the lowest drop of 64.9 °C (Fig. 5d), which was the best catalytic performance among all shelled spheres investigated here. It is easy to explain that the best catalytic performance from the double-shelled hollow spheres should be attributed to their largest specific surface area.

The dependence of AP decomposition on different contents of the double-shelled $NiCo_2O_4$ hollow spheres was studied using DSC tests, as displayed in Fig. 6. The thermal decomposition process of AP changed obviously on increasing the addition of the double-shelled $NiCo_2O_4$ hollow spheres (Fig. 6). According to the analyses of the DSC data, the double-shelled $NiCo_2O_4$ hollow spheres showed negligible effects on the temperature of the crystal transition during the process of AP thermal decomposition. All incorporations of different contents of the double-shelled $NiCo_2O_4$ hollow spheres could lead to a more or less decrease in both the LTD and HTD peak temperatures of AP. When the weight percent of the double-shelled $NiCo_2O_4$ hollow spheres was 1 wt%, the LTD and HTD peak temperatures decreased to 280.5 °C and 366.4 °C, respectively. On increasing the content of double-shelled hollow spheres till 10 wt%, the HTD peak temperature of AP was reduced gradually from 366.4 °C (Fig. 6b) to *ca.* 320.0 °C (Fig. 6f–g). Furthermore, the NiO microspheres, which were previously reported as the catalyst for the thermal decomposition of AP, could just reduce the HTD peak of AP from 460.0 °C to 386.0 °C.[45] Deng and co-workers adopted the Ni–P alloy sample as a catalyst, which made the HTD peak of AP locate in the range from 340.0 °C to 394.0 °C.[46] The LTD peak of AP disappeared when the content of the double-shelled hollow spheres was more than 6 wt%. Compared with neat AP, the double-shelled hollow spheres decreased the HTD peak temperature by 94.0 °C when the content was 8 wt%. It can be concluded that the double-shelled $NiCo_2O_4$ hollow spheres remarkably promote the AP decomposition with a considerable reduction in their decomposition temperatures. However, when the quantity

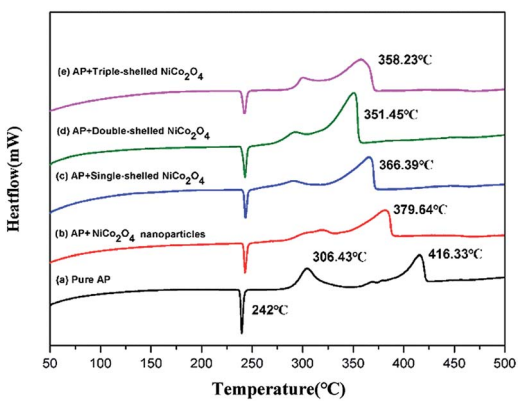

Fig. 5 The DSC curves of the AP decomposition in the absence and presence of different layer numbers of $NiCo_2O_4$ hollow spheres: (a) neat AP, (b) AP + $NiCo_2O_4$ nanoparticles, (c) AP + single-shelled $NiCo_2O_4$, (d) AP + double-shelled $NiCo_2O_4$, (e) AP + triple-shelled $NiCo_2O_4$.

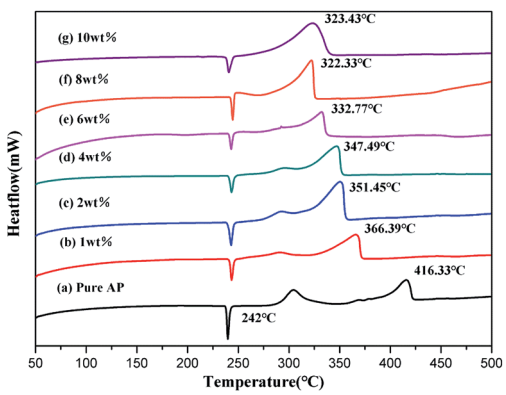

Fig. 6 The dependence of the AP decomposition examined by DSC curves on the different amounts of double-shelled $NiCo_2O_4$ hollow spheres: (a) neat AP, (b) AP + $NiCo_2O_4$-1wt%, (c) AP + $NiCo_2O_4$-2wt%, (d) AP + $NiCo_2O_4$-4wt%, (e) AP + $NiCo_2O_4$-6wt%, (f) AP + $NiCo_2O_4$-8wt%, (g) AP + $NiCo_2O_4$-10wt%.

of double-shelled $NiCo_2O_4$ hollow spheres increased to a certain extent, their catalytic activity weakened as a result of the reduction in their specific surface area and active sites. Meanwhile, the reduction trend for the peak temperature of AP was gradually maintained.[3,47,48]

3.4 Catalytic mechanism for the multi-shelled $NiCo_2O_4$ hollow spheres on AP

The decomposition process of AP is a solid–gas multiphase reaction.[49] At a relatively low temperature range, AP initially decomposes into a small amount of intermediates, some of which further dissociate and sublimate to form NH_3 and $HClO_4$:

$$NH_4ClO_4(s) \rightarrow ClO_4^- + NH_4^+ \rightarrow HClO_4(s) + NH_3(s) \rightarrow HClO_4(g) + NH_3(g)$$

However, the reaction could not be completed between the intermediate products NH_3 and $HClO_4$ since the unreacted NH_3 was adsorbed on the surface of AP. When the surface of AP was entirely covered with NH_3, the decomposition reaction of AP was suspended (Fig. 7). As the temperature continued to rise, the absorbed NH_3 on the AP surface started to react with $HClO_4$ again, thus resulting in the formation of volatile products.[50]

When the multi-shelled $NiCo_2O_4$ hollow spheres were added as a catalyst, due to an unfilled orbit from the composite transition metal oxides, ClO_4^- could be easily accepted and transferred to the surface of the catalyst. Subsequently, NH_4^+ could accept an electron to decompose into NH_3 and ClO_4^- was converted to $HClO_4$. At this point, the presence of Co^{2+}/Co^{3+}, Ni^{2+}/Ni^{3+} and Co^{3+}/Ni^{2+}, located on the surfaces of $NiCo_2O_4$ lattices as the active sites for reduction, could trigger electron transfers and provide channels for electron transfers for catalytic reactions. The reaction process can be described as follows:[51–53]

$$Ni^{3+} + ClO_4^- \rightarrow Ni^{2+} + ClO_4^0$$

$$Co^{2+} + NH_4^+ \rightarrow Co^{3+} + NH_4^0$$

$$Ni^{2+} + NH_4^+ \rightarrow Ni^{3+} + NH_4^0$$

$$Co^{3+} + ClO_4^- \rightarrow Co^{2+} + ClO_4^0$$

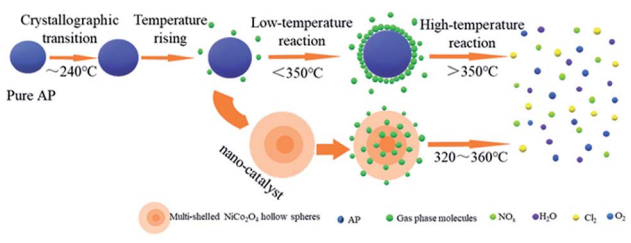

Fig. 7 The schematic diagram of the thermal decomposition process of AP in the absence and presence of the multi-shelled $NiCo_2O_4$ hollow spheres.

In addition, the gaseous intermediates, which were produced during the thermal decomposition of AP, were adsorbed onto the surfaces of the multi-shelled composite metal oxide hollow spheres as a result of their high specific surface area and high adsorption capacity (Fig. 7). This led to a considerable increase in the active sites and contact areas for the catalytic reaction, which further guaranteed its continuation. Finally, the gaseous intermediates, which were adsorbed initially on the surfaces of the multi-shelled $NiCo_2O_4$ hollow spheres, were desorbed from pore walls immediately after the electron transfer on the active sites to form final products such as HCl, H_2O, Cl_2, O_2, NO, N_2O and NO_2. Therefore, the multi-shelled $NiCo_2O_4$ hollow spheres showed more excellent catalytic capabilities than $NiCo_2O_4$ nanoparticles.

4. Conclusions

In conclusion, multi-shelled $NiCo_2O_4$ hollow spheres were prepared by a facile hydrothermal–calcination method with smooth surfaces and uniform particle sizes. The catalytic results from our designed experiments revealed that the multi-shelled $NiCo_2O_4$ hollow spheres displayed a remarkable catalytic effect on the thermal decomposition of AP due to their special structure with a large specific surface area, numerous active sites for reduction and strong adsorption capacity. Furthermore, the $NiCo_2O_4$ hollow spheres demonstrated better catalytic activity than the $NiCo_2O_4$ nanoparticles in the same test conditions. In the end, a mechanism was proposed based on the electron transfer processes for AP decomposition in the presence of the prepared $NiCo_2O_4$ hollow spheres.

Conflicts of interest

The authors declare that they have no conflict of interest.

Acknowledgements

This research was supported by the National Natural Science Foundation of China (Grant 51576101), Qing Lan Project and the Fundamental Research Funds for the Central Universities (Grant 30918015102).

References

1 J. F. Guery, I. S. Chang, T. Shimada, M. Glick, D. Boury, E. Robert, J. Napior, R. Wardle, C. Perut, M. Calabro, R. Glick, H. Habu, N. Sekino, G. Vigier and B. d'Andrea, *Acta Astronaut.*, 2010, **66**, 201–219.
2 L. R. Paulina, P. Paula, C. C. Christopher, L. A. Juan, M. V. Cesar, A. Gabriel and B. C. María, *RSC Adv.*, 2019, **9**, 8480–8489.
3 S. G. Hosseini, R. Ahmadi, A. Ghavi and A. Kashi, *Powder Technol.*, 2015, **278**, 316–322.
4 M. Zou, X. H. Jiang, L. Lu and X. Wang, *J. Hazard. Mater.*, 2012, **225**, 124–130.
5 V. V. Boldyrev, *Thermochim. Acta*, 2006, **443**, 1–36.

6 H. Xu, X. B. Wang and L. Z. Zhang, *Powder Technol.*, 2008, **185**, 176–180.
7 Y. Zhao, X. Zhang, X. Xu, Y. Zhao, H. Zhou, J. Li and H. B. Jin, *CrystEngComm*, 2016, **18**, 4836–4843.
8 W. Wang and D. Zhang, *RSC Adv.*, 2018, **8**, 32221–32230.
9 D. Jing, D. Chen, G. Fan, Q. Zhang, J. Xu, S. Gou, H. Li and F. Nie, *Cryst. Growth Des.*, 2016, **16**, 6849–6857.
10 Y. Lan, X. Li, G. Li and Y. Luo, *J. Nanopart. Res.*, 2015, **17**, 1–9.
11 G. Li and W. Y. Bai, *Chem. Phys.*, 2018, **506**, 45–51.
12 M. A. Fertassi, K. T. Alali, Q. Liu, *et al.*, *RSC Adv.*, 2016, **6**, 74155–74161.
13 L. N. Jin, Q. Liu and W. Y. Sun, *CrystEngComm*, 2012, **14**, 7721–7726.
14 S. S. Lu, X. Y. Jing, J. Y. Liu, J. Wang, Q. Liu, Y. H. Zhao, S. Jamil, M. L. Zhang and L. H. Liu, *J. Solid State Chem.*, 2013, **197**, 345–351.
15 Y. J. Zhao, X. M. Xu, Y. Z. Zhao, H. P. Zhou, J. B. Li and H. B. Jin, *J. Alloys Compd.*, 2016, **654**, 523–528.
16 M. H. Oh, T. Yu, S. H. Yu, B. Lim, K. T. Ko, M. G. Willinger, D. H. Seo, B. H. Kim, M. G. Cho, J. H. Park, K. Kang, Y. E. Sung, N. Pinna and T. Hyeon, *Science*, 2013, **340**, 964–968.
17 J. B. Joo, Q. Zhang, M. Dahl, I. Lee, J. Goebl, F. Zaera and Y. D. Yin, *Energy Environ. Sci.*, 2012, **5**, 6321–6327.
18 J. Wang, H. Ren, W. F. Chen, P. Koshy and C. C. Sorrell, *Ceram. Int.*, 2018, **44**, 4981–4989.
19 S. Hyuk Im, U. Jeong and Y. N. Xia, *Nat. Mater.*, 2005, **4**, 671–675.
20 J. Liu, S. Z. Qiao, S. Budi Hartono and G. Q. Lu, *Angew. Chem., Int. Ed.*, 2010, **49**, 4981–4985.
21 K. An and T. Hyeon, *Nano Today*, 2009, **4**, 359–373.
22 Z. Y. Wang, D. Y. Luan, F. Y. C. Boey and X. W. Lou, *J. Am. Chem. Soc.*, 2011, **133**, 4738–4741.
23 Y. J. Hong, M. Y. Son and Y. C. Kang, *Adv. Mater.*, 2013, **25**, 2279–2283.
24 X. W. Lou, L. A. Archer and Z. C. Yang, *Adv. Mater.*, 2008, **20**, 3987–4019.
25 S. M. Xu, C. M. Hessel, H. Ren, R. B. Yu, Q. Jin, M. Yang, H. J. Zhao and D. Wang, *Energy Environ. Sci.*, 2014, **7**, 632–637.
26 Z. H. Dong, H. Ren, C. M. Hessel, J. Y. Wang, R. B. Yu, Q. Jin, M. Yang, Z. D. Hu, Y. F. Chen, Z. Y. Tang, H. J. Zhao and D. Wang, *Adv. Mater.*, 2014, **26**, 905–909.
27 X. Y. Lai, J. Li, B. A. Korgel, Z. H. Dong, Z. M. Li, F. B. Su, J. Du and D. Wang, *Angew. Chem., Int. Ed.*, 2011, **50**, 2738–2741.
28 L. F. Shen, L. Yu, X. Y. Yu and X. G. Zhang, *Angew. Chem., Int. Ed.*, 2015, **54**, 1868–1872.
29 Z. Wang, W. Jia, M. L. Jiang and C. Che, *Nano Res.*, 2016, **9**, 2026–2033.
30 L. Li, R. Z. Ma, N. Iyi, Y. Ebina and K. Takada, *Chem. Commun.*, 2006, 3125–3127.
31 Y. Zeng, X. Wang, H. Wang, Y. Dong and Y. Ma, *Chem. Commun.*, 2010, **46**, 4312–4314.
32 J. Qi, K. Zhao, G. D. Li, Y. Gao, H. J. Zhao, R. B. Yu and Z. Y. Tang, *Nanoscale*, 2014, **6**, 4072–4077.
33 P. F. Xu, R. B. Yu, H. Ren, L. B. Zong, J. Chen and X. R. Xing, *Chem. Sci.*, 2014, **5**, 4221–4226.
34 J. Y. Wang, N. L. Yang, H. J. Tang, Z. H. Dong, Q. Jin, M. Tang, D. Kisailus, H. J. Zhao and Z. Y. Tang, *Angew. Chem., Int. Ed.*, 2013, **125**, 6545–6548.
35 E. Alizadeh-Gheshlaghi, B. Shaabani, A. Khodayari, Y. Azizian-Kalandaragh and R. Rahimi, *Powder Technol.*, 2012, **217**, 330–339.
36 L. F. Shen, L. Yu, X. Y. Yu, X. G. Zhang and X. W. Lou, *Angew. Chem., Int. Ed.*, 2015, **54**, 1868–1872.
37 X. X. Sun and Y. D. Li, *Angew. Chem., Int. Ed.*, 2004, **43**, 597–601.
38 M. Thommes, *Chem. Ing. Tech.*, 2010, **82**, 1059–1073.
39 M. Kruk and M. Jaroniec, *Chem. Mater.*, 2001, **13**, 3169–3183.
40 Y. Wang, C. Zhao, W. Fu, Z. Zhang, M. Zhang, J. Zhou and E. Xie, *J. Alloys Compd.*, 2016, **668**, 1–7.
41 D. Su, Y. Zhao, R. Zhang, M. Ning, Y. Zhao, H. Zhou, J. Li and H. Jin, *Appl. Surf. Sci.*, 2016, **389**, 112–117.
42 E. A. Campos, M. T. Cortez Fernandes, E. Y. Kawachi, J. I. Sampaio de Oliveira and R. Lazzarini Dutra, *Propellants, Explos., Pyrotech.*, 2015, **40**, 860–866.
43 L. M. Zhou, H. Y. Liu and F. S. Li, *Acta Phys.-Chim. Sin.*, 2006, **22**, 627–630.
44 J. X. Wang, W. C. Zhang, Z. L Zheng, Y. Gao, K. F. Ma, J. H. Ye and Y. Yang, *J. Alloys Compd.*, 2017, 720–727.
45 J. J. Wang, C. Z. Wei, H. Pang, F. Gao, J. Z. Yin, L. Guan and Q. Y. Lu, *Catal. Commun.*, 2011, **12**, 1031–1036.
46 Y. Deng, Y. Y. Yang, L. Y. Ge, W. Z. Yang and K. N. Xie, *Appl. Surf. Sci.*, 2017, **425**, 261–271.
47 N. Li, Z. F. Geng, M. H. Cao, L. Ren, X. Y. Zhao, B. Liu, Y. Tian and C. W. Hu, *Carbon*, 2013, **54**, 124–132.
48 T. Liu, L. S. Wang, P. Yang and B. Y. Hu, *Mater. Lett.*, 2008, **62**, 4056–4058.
49 Y. Wang, X. Xia, J. Zhu, Y. Li, X. Wang and X. Hu, *Combust. Sci. Technol.*, 2010, **183**, 154–162.
50 Y. F. Lan, M. M. Jin and Y. J. Luo, *J. Sol-Gel Sci. Technol.*, 2015, **74**, 161–167.
51 T. Liu, L. Wang, P. Yang and B. Hu, *Mater. Lett.*, 2008, **62**, 4056–4058.
52 N. M. Juibari and A. Eslami, *J. Therm. Anal. Calorim.*, 2017, **128**, 115–124.
53 Y. Liang and G. Li, *Mater. Res. Express*, 2019, **6**, 0850e8.